Point defects and clustering in uranium dioxide by LSDA+U calculations

Hua Y. Geng, Ying Chen, and Yasunori Kaneta

Department of Quantum Engineering and Systems Science, The University of Tokyo, Hongo 7-3-1, Tokyo 113-8656, Japan

Misako Iwasawa and Toshiharu Ohnuma

Materials Science Research Laboratory, Central Research Institute of Electric Power Industry, Tokyo 201-8511, Japan

Motoyasu Kinoshita

Nuclear Technology Research Laboratory, Central Research Institute of Electric Power Industry, Tokyo 201-8511, Japan
and Japan Atomic Energy Agency, Ibaraki 319-1195, Japan

A comprehensive investigation on point defects and their clustering behavior in nonstoichiometric uranium dioxide $UO_{2\pm x}$ is carried out using the LSDA+U method based on density functional theory. Accurate energetic information and charge transfers available so far are obtained. With these energies that have improved more than 50% over that of pure generalized gradient approximation and local density approximation, we show that the density functional theory predicts the predominance of oxygen defects over uranium ones at any compositions, which is possible only after properly treating the localized $5f$ electrons. Calculations also suggest an upper bound of $x \sim 0.03$ for oxygen clusters to start off. The volume change induced by point uranium defects is monotonic but nonlinear, whereas for oxygen defects, increasing x always reduces the system volume linearly, except dimers that require extra space for accommodation, which has been identified as a metastable ionic molecule. Though oxygen dimers usually occupy Willis O'' sites and mimic a single oxygen in energetics and charge state, they are rare at ambient conditions. Its decomposition process and vibrational properties have been studied carefully. To a general clustering mechanism in anion-excess fluorites systematically obtain, we also analyze the local stabilities of possible basic clustering modes of oxygen defects. The result shows a unified way to understand the structure of Willis-type and cuboctahedral clusters in UO_{2+x} and β-U_4O_9. Finally, we generalize the point defect model to the independent cluster approximation to include clustering effects; the impact on defect populations is discussed.

I. INTRODUCTION

Oxides of the fluorite structure include ZrO_2, which is a common ceramic in research and industry, CeO_2, and the actinide oxides ThO_2, UO_2, and PuO_2. The series of actinide dioxides is of great interest in nuclear applications. The present generation of nuclear reactors uses UO_2 as nuclear fuel. Fast breeder reactors at present employ mixed $(U, Pu)O_2$ and may use $(U, Th)O_2$ in the future. In the oxides of the fluorite or CaF_2 structure, MO_2, each metal atom M is surrounded by eight equivalent nearest-neighbor O atoms, each of which is in turn surrounded by a tetrahedron of four equivalent M atoms. A typical feature of the fluorite structure is the large $(\frac{1}{2}, \frac{1}{2}, \frac{1}{2})$ octahedral holes in which interstitial ions can easily be accommodated. Fluorite structure of UO_2 transforms to an orthorhombic *Pnma* phase under a hydrostatic compression beyond 40 GPa, which is in turn followed by an isostructural transition after 80 GPa.[1,2] At ambient pressure, however, it exists as the single phase stoichiometric oxide at all temperature up to 2073 K. Above that, it transforms to the substoichiometric phase UO_{2-x}, whereas at lower temperatures, it easily dissolves large amounts of interstitial oxygen to form *anion-excess* compositions UO_{2+x}. Higher interstitial concentration leads to another ordered phase, U_4O_9, which closely relates to the fluorite structure.[3] It was argued that stoichiometric U_4O_9 does not exist and should actually be U_4O_{9-y}.[4] However, for simplicity we still use U_4O_9 to refer

to the nonstoichiometric phase hereinafter. There are three polymorphs of U_4O_9 between room temperature and 1273 K, which are known as α, β, γ, where the α/β boundary is at 353 K and the β/γ boundary is at about 873 K. Only the detailed atomic arrangement in β phase is clearly determined: the excess anions accommodate in *cuboctahedral clusters* centered on the 12-fold sites of the cubic space group $I\bar{4}3d$, where the uranium sublattice remains *undisturbed*.[4,5] Although the unit cell is 64 times larger than a normal cubic fluorite cell, the *average cell* is still in fluorite type except that one has to introduce some vacancies at normal anion sites and two types of interstitial oxygen, each of which is sited about 1 Å from the empty octahedral site of the fcc cation sublattice along $\langle 110 \rangle$ (O') and $\langle 111 \rangle$ (O'') directions, respectively. This characteristic is also shared by the α phase[6] and UO_{2+x},[7,8] with the difference that U_4O_9 has a long-range ordering for the interstitial oxygen atoms while in UO_{2+x} it is just short range ordered. To prevent some oxygens from being too close to each other, an intuitive proposal that different kinds of oxygen defects are associated to form *defect clusters* is widely adopted when modeling these phases.[7,8]

At first sight, the fact that interstitials were detected not at the body centers of the cubic interstitial sites but at sites considerably displaced from this symmetric position is puzzling. In rare earth doped alkaline earth fluorides, it has been conclusively shown that at low interstitial concentrations

(1 mole % or less), the anions occupy the symmetric body center interstitial site, but usually the low-symmetry defect structure is a general feature of anion-excess fluorites.[9] About half a century has elapsed, people still know few about the stabilization mechanism of Willis O′ and O″ sites in energetics. In the limit of $x \rightarrow 0$ in UO_{2+x}, whether the excess-anions will occupy the octahedral interstitial site or not is still *unclear*. On the other hand, though the occurrence of cuboctahedral clusters in β-U_4O_9 has been confirmed by experiments, the geometry of defect clusters in the low interstitial concentration regime is unknown. One of the simplest model is to assume that the Willis 2:2:2 cluster (see Ref. [8] for its geometry) can exist independently and distribute randomly in the material around this concentration. Allen *et al.*[10] proposed a model for U_4O_9 in this line by chaining 2:2:2 clusters along the $\langle 110 \rangle$ direction. Unfortunately, his model is definitely wrong because the inconsistencies with the following experimental facts: (i) it leads to an exact stoichiometric U_4O_9, which might not exist, (ii) no cuboctahedral clusters can be formed in his arrangement, and (iii) it has an equal concentration for O′ and O″ sites against the measurements that O″ position has a much lower occupancy.[4,5]

Therefore, an investigation of the geometry and stability of possible defect clusters with a first principles method is required, but it is never easy. The big unit cell of U_4O_9 and the shortage of information about the atomic arrangement in UO_{2+x} have restricted most attempts within *point defect* approximation, and only the formation energy of simple intrinsic defects (Frenkel pairs and Schottky defect) was calculated.[11–13] Applying these energies to the point defect model (PDM),[14,15] however, did not produce satisfactory *defect populations*—uranium vacancy dominates in the hyperstoichiometric regime against the experimental anticipation.[12,13] The failure might be attributed to the limitation of the PDM, which assumes isolated noninteracting point defects, whereas in UO_{2+x} this is impossible when $x \geq 0.03$, as we will show later. Also, it can arise from the inaccurate energies produced by the local density approximation (LDA) or the generalized gradient approximation (GGA) of the electronic density functional that has been proven to fail to describe *localized states*.[2] Nevertheless, some qualitative properties can still be accessed by static calculations within this model. For example, the diffusion rate of interstitials can be simply modeled by estimating the migration energy along all possible paths that bridge the initial and finial interstitial positions, which is readily computable by the *ab initio* nudged elastic band (NEB) algorithm. For UO_{2+x}, the conclusion is that a direct diffusion is almost prohibited and a normal oxygen on the fluorite lattice site must be involved as an intermediate process. That is, the interstitial atom pushes a neighboring lattice oxygen into another interstitial site and itself jumps into the vacancy thus created (*interstitialcy* mechanism).[16] The extreme of this process is that it evidently creates a transient oxygen dimer and thus sets up an *upper bound* to the migration energy for thermodynamic diffusion of oxygens. In order to keep the occurrence probability of oxygen dimer to be consistent with the experimental observation in bulk U_4O_9,[17] the energy required to form such a kind of dimer should be much larger than the average migration energy. However, this has not yet been confirmed by *ab initio* calculations. Near the surface of UO_2 that is exposed to air, however, oxygen dimer might prevail due to *oxidations*. Moreover, their stability in UO_2 matrix may shed some light on the mechanism of how the material dissolves O_2 molecules into individual interstitials. Also, it verifies the Willis assumption that *each O″ interstitial has to be associated with one vacancy that occupies the nearest oxygen site*[7] since, otherwise, they must form an oxygen dimer.

These motivate the research work of this paper that mainly focuses on (i) the stability of isolated point oxygen interstitial in UO_{2+x} when $x \rightarrow 0$, (ii) the stability and decomposition process of oxygen dimer including the variations of energy, cell volume, and charges, and (iii) the local stability of defect clusters that is composed of oxygen vacancies and O′ and O″ interstitials. These clusters can be viewed as fractal pieces of a cuboctahedral cluster, which is essential in the U_4O_9 phase. It is believed that the transition from UO_{2+x} to U_4O_9 involves *long-range ordering* of the defect complexes, leading to a change in the symmetry relating the relative positions of the complexes, without producing any atomic rearrangement within these complexes, i.e., microdomains of U_4O_9 should already exist in UO_{2+x}.[7] What we also want to find out primarily in this paper is the kind of cluster that is the most possible candidate for this complex and its polymorphs when x is increased. In the next section, we will discuss the calculation method. Main results and discussions are presented in Sec. III. The formation energy analysis is discussed in Sec. III B and the charge transfer is discussed in Sec. III C. In Secs. III D and III E, we will discuss the properties of oxygen dimer in UO_2 and its decomposition process. The defect clustering pattern and its tendency with increased x are given in Sec. III F, while in Sec. III G a generalization of PDM including clustering effects is proposed, as well as the associated defect population analysis. Finally, in Sec. IV we summarize the paper.

II. METHOD OF CALCULATION

Our investigation in the defective behavior of UO_2 is based on a series of total energy calculations with different configurations in fluorite structure, which varied in simulation cell size and defect arrangement. The plane-wave method using density functional theory (DFT) to treat the electronic energy as implemented in the VASP code[18,19] was employed, as well as the projector-augmented wave pseudopotentials.[20,21] The $2s^2 2p^4$ electrons in oxygen and $6s^2 6p^6 5f^3 6d^1 7s^2$ electrons in uranium were treated in valence space. The cutoff for the kinetic energy of plane waves was set as high as 500 eV to eliminate the possible Pulay stress error. Also, it has been increased due to the presence of oxygen, which requires an energy cutoff at least 400 eV to converge the electronic energy within a few meV. Integrations over reciprocal space were performed in the irreducible Brillouin zone with about 8–36 nonequivalent k points, depending on the system size. The energy tolerance for charge self-consistency convergence was set to 1×10^{-5} eV for all calculations. Moreover, the total convergence of this parameter set was checked well. Without a specific statement, all

structures in the following discussions have been fully relaxed to get all Hellman–Feynman forces (stress) less than 0.01 eV/Å.

The electronic exchange-correlation energy was computed by spin-polarized local density approximation with an effective on-site Coulomb interaction to split the partially filled $5f$ bands localized on uranium atoms (LSDA+U).[22,23] Parameters of the Hubbard term were taken as $U=4.5$ eV and $J=0.51$ eV, which have been checked carefully for *fluorite* UO_2.[2,24–26] Here, some comments are desired. It is well known that it is the U but J that sensitively contributes to the electronic structure. In the UO_2 case, the value of U quite depends on the atomic arrangement of uranium atoms.[2] If the uranium sublattice is almost unchanged, which is the case here, one can expect that U would not vary too much. On the other hand, the influence of interstitial oxygens on localized $5f$ electrons should be small if they are well separated from uranium atoms. However, as the interstitial concentration increased, the impact on U may become non-negligible. Therefore, we must restrict to a certain composition regime and $x \leq 0.25$ should be small enough to allow us to use this set of parameters. This composition value can be roughly estimated by checking the induced deformation on the uranium sublattice. The situation of uranium defects is a little embarrassing. We cannot estimate its effect on U until a more accurate functional becomes generally available, for example, the hybrid density functional that has shown impressive versatility in preliminary applications.[27] However, for a point defect in a large enough cell, neglecting this influence seems reasonable. Another point is about the adoption of LSDA+U functional instead of GGA+U. The latter has been proven as of a poor description to the defect energetics, which we will discuss in detail in Sec. III G.

The *supercell* method has been used to model defect structures. Periodic boundary conditions were imposed on the whole system. The geometries of all structures (except those in Sec. III F) are listed in Table I, where each brick indicates a fluorite cubic unit cell (in U_4O_8) and red points represent oxygen interstitials, which usually occupy the cubic centers, except those associated with dimers. Dot-lined box (if drawn) indicates the oxygen cage. No atom on the fluorite lattice has been drawn explicitly, except in $C4_{1d}$ and $C4_{1d1}$ where the lattice oxygens bonded to interstitials were also plotted. Each structure of $C4_{1d}$, $C4_{2d}$, and $C4_{1d1}$ contains one oxygen dimer. Configuration $^uC8_1$ has the same geometry as $C8_1$ but replacing the interstitial oxygen with one uranium, and $^uC8_{-1}$ or $C8_{-1}$ corresponds to remove one lattice atom from a system with eight fluorite cubic cells ($2 \times 2 \times 2$).

The magnetic effects have been taken into account by initially setting up an *antiferromagnetic* orientation of atomic moments. Two cases, the moment ordering along the longest (L) and the shortest (S) axis, are considered. The cohesive energy E_{coh} of each structure is calculated from the total energy by subtracting the isolated spin-polarized atomic contributions. Then, the oxygen defect formation energy in structure Cm_n is given by

$$E_f = E_{coh} - mE_{coh}^{C1} - \frac{n}{2}E_{O_2}. \tag{1}$$

Here, m is the number of fluorite cubic cells and n is the total oxygen interstitials or vacancies. E_{O_2} is the binding energy of a neutral dioxygen molecule. Alternatively, one can define an *alloy-system* such as formation energy by choosing $C1_1$ as one of the reference phases instead of O_2 molecule. We call it the *relative formation energy*, which explicitly takes the advantage of showing the phase stability of superstructures with different compositions, analogous to that in an alloy and compound system.[28,29] It can thus be calculated as

$$E_{Rf} = E_{coh} - \left(1 - \frac{n}{m}\right)E_{coh}^{C1} - \frac{n}{m}E_{coh}^{C1_1}, \tag{2}$$

and the value of n/m stands for the composition of phase $C1_1$ in $C1$ or, equivalently, the concentration of oxygen interstitial per fluorite cubic cell. All configurations incorporated with uranium defect are marked by a superscript u in Table I, and the formation energy for a defect in ^uCm_n is defined as

$$E_f = E_{coh} - mE_{coh}^{C1} - nE_{\alpha U}. \tag{3}$$

Here, $E_{\alpha U}$ is the cohesive energy per atom in the metallic α-U phase, and we use the experimental value of -5.4 eV for simplicity.[30]
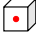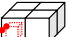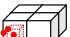
Vibrational frequencies of interstitial oxygens were calculated by finite difference method with *frozen phonon* approximation. At finite temperatures, these vibrational frequencies directly contribute to the first order of defect free energy, which is given by $F(T) = E_f - \kappa_B T \ln Z_v$, with the partition function

$$Z_v = \prod_i \sum_{j=0}^{\infty} \exp\left(\frac{-E_j^i}{\kappa_B T}\right), \tag{4}$$

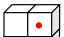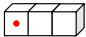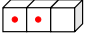where κ_B is the Boltzmann constant and E_j^i is the eigenvalue energy for the jth vibrational mode with frequency ω^i, and the harmonic approximation $E_j^i = \hbar\omega^i(j+\frac{1}{2})$ has been used. Here, we have not subtracted the vibrational free energy of the reference state O_2 molecule and comparison of the calculated free energies can therefore be made only among configurations with the *same* number of interstitial oxygens.

Regarding charge transfer calculations, it is well known that the concept of static atomic charge in *ab initio* calculations usually leads to ambiguity due to the arbitrariness in determining the belongingness of electrons. Nevertheless, there are several methods that exist to compute the effective atomic charge, which provide some useful qualitative understanding. Among those, Bader's conception, which partitions an electronic density by surfaces formed by the density minima (zero flux surfaces), is one of the most intuitive. It is simple to calculate Bader charges, requiring only atomic positions and electronic density as input. The partition surfaces are determined by finding the charge density minima.[31] Then, the atomic charge is obtained by subtracting the valence electrons from the integral of charge density over the space surrounded by the partition surfaces that envelops the atom. Another widely used concept is the dynamical effec-

TABLE I. Equilibrium properties of uranium dioxide with defects: superscript u denotes uranium defects and negative subscript refers to vacancy. ΔV is the volume difference relative to the $C1$ structure and E_f is the defect formation energy per point defect. Note that $\bar{E}_{coh}$ and volume have been averaged to a single fluorite cubic cell.

Label	$\bar{E}_{coh}$ (eV/cell)	Volume (Å^3/cell)	ΔV (Å^3/cell)	E_f (eV)	Structure
$C1$	−98.638	161.34	0.0	0.0	
$C1_1$	−102.906	157.17	−4.17	−1.394	
$C2_1(L/S)$	−101.20/−101.199	159.47/159.46	−1.87/−1.88	−2.249/−2.248	
$C4_1(L/S)$	−99.71/−99.731	160.54/160.28	−0.8/−1.06	−1.413/−1.496	
$C4_{1d}(S)$	−99.337	162.87	1.53	0.079	
$C4_{2d}(S)$	−100.486	163.05	1.71	−1.642[a]	
$C4_{1d1}(S)$	−100.461	162.09	0.75	−1.545[a]	
$C4_2(L/S)$	−101.233/−101.237	159.35/159.38	−1.99/−1.96	−2.316/−2.324	
$C8_1$	−99.268	161.05	−0.29	−2.169	
$C3_1^L(L/S)$	−100.099/−100.361	160.25/160.16	−1.09/−1.18	−1.509/−2.294	
$C3_2^L(L/S)$	−101.789/−101.788	159.34/159.36	−2.0/−1.98	−1.853/−1.850	
$C8_{-1}$	−97.338	161.54	0.20	7.525	
$^uC8_1$	−98.289	164.25	2.91	8.194	
$^uC8_{-1}$	−96.831	160.26	−1.08	9.056	

[a]Per two oxygen interstitials.

tive charge defined by the change of polarization induced by atomic displacements,[32] which is beyond the scope of this paper and will not be elaborated here.

III. RESULTS AND DISCUSSIONS

A. Dioxygen molecule

First, we discuss the dioxygen molecule. The O_2 molecule was modeled by putting it in a periodic cubic cell with a lattice constant of 15 Å, which is large enough to eliminate the factitious interaction among its images. Only one k point (Γ) was used. Since the notorious failure of LDA in describing small isolated molecules, we employed here (and only here) the revised Perdew–Burke–Ernzerhof[33] GGA electronic exchange-correlation functional. The bond length was optimized to be 1.22 Å, which is in good agreement with the experimental value of 1.21 Å.[34,35] The calculated binding energy is −5.75 eV, which is a little deeper than the observed value of −5.1 eV.[36] This discrepancy should attribute to the difficulty of the current functional to accurately take into account the van der Waals interactions. The vibrational fre-

quency of stretch mode, however, was well reproduced as 1588.6 cm^{-1} against the experimental value of 1580.2 cm^{-1}.[34] As a check to the validity of Bader's conception, we calculated the Bader atomic charge for each oxygen atom in O_2 and got them as $\pm 0.09e$, which reflects the essential of *covalent* bond correctly. The deviation can be reduced further when it is in an ionic bond environment where the charge density minimum surfaces sharply show up.

B. Structure and formation energies

1. Oxygen interstitials

The calculated equilibrium properties of 14 configurations, including cohesive energies, equilibrium volumes, volume changes relative to the ideal UO_2 cell, and defect formation energies, are listed in Table I. These data have been *averaged* to one fluorite cubic cell. It can be seen that the cohesive energy always decreases as the oxygen interstitial concentration increases, demonstrating the tendency of uranium dioxide to dissolve oxygens. The solubility, however, cannot be determined by simply taking the limit of this cohesive energy vs concentration curve. Also, the relative sta-
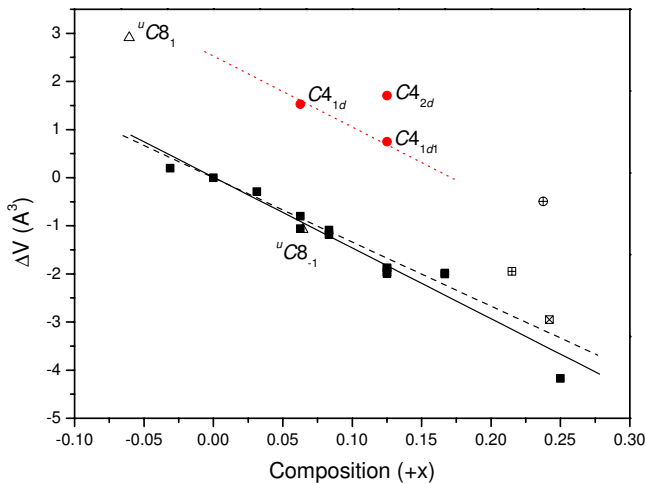
FIG. 1. (Color online) Calculated variation of the volume change in UO_{2+x} with the deviation from stoichiometry x. Solid squares are point oxygen defects and the solid line is the linear fitting to them. Open triangles are for uranium defects. Solid circles are those incorporated with one oxygen dimer; the dotted line is for eye guide. Experimental data: Dashed line is for UO_{2+x} reported by McEachern and Taylor and others for β-U_4O_9 [at room temperature (⊠), 503 K (⊞), and 773 K (⊕)].
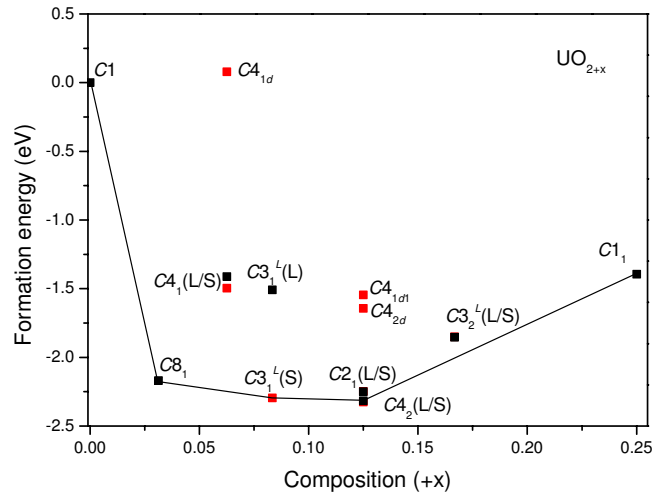

FIG. 2. (Color online) Formation energy of oxygen interstitials in UO_2 arranged in various configurations. $C8_1$ corresponds to an isolated defect approximation and other configurations must be interpreted as ordered defect phases.

bility among different configurations has been obscured here. To get that information explicitly, one needs to return to the relative formation energy.

One interesting thing is that we find, except that of the oxygen dimer, that introducing point oxygen interstitials always shrinks the system, i.e., leads to a *negative* ΔV, as shown in Fig. 1. This feature differs from GGA results,[13] but agrees with GGA+U,[37] and may attribute to the behavior of localized $5f$ electrons. Generally, a negative ΔV means that the interaction between the matrix and the interstitials is dominated by attractive chemical potentials rather than by mechanical effects (atomic *size effect*). The latter always results in a swollen volume and is important for big interstitial atoms or inert gases. Oxygen dimer belongs to this class and requires extra space to accommodate, which can be seen more clearly when comparing $C4_{1d}$ with $C4_1$ and $C4_{1d1}$ configurations. The influence of magnetic orientation on equilibrium volume is almost negligible except in the cases of $C4_1$ and $C3_1^L$, of which only $C3_1^L$ has a notable formation energy difference between L and S orientation.

The calculated slope of volume variation induced by oxygen interstitials (the solid line in Fig. 1) is in good agreement with experimental change of the lattice constant $a = 5.4696 - 0.1495x$, as reported by McEachern and Taylor for homogenous UO_{2+x} powders as quoted in Ref. 38 (the dashed line). Also, it is in accord with the volume change of β-U_4O_9 measured at room temperature[17] with respect to that of stoichiometric UO_2.[1] Increase temperature to 503 and 773 K expands the material greatly,[5] which can be understood in terms of thermal vibration effects and extensive defect generation.

Figure 2 shows the defect formation energies of oxygen interstitial in all considered configurations of UO_{2+x} within $0 \leq x \leq 0.25$. Note that the values of $C4_{2d}$ and $C4_{1d1}$ are for

two interstitials. A remarkable feature in this graph is that in *energetics*, an oxygen dimer mimics a single oxygen atom. Comparing that of the perfect crystal $C1$ with $C4_{1d}$ and that of $C4_1$ with $C4_{2d}$ and $C4_{1d1}$, we see that despite the fact that the latter contains one more interstitial, the formation energy is almost the same. This means that absorbing an oxygen from O_2 gas into UO_2 and forms a dimer will neither release nor gain heat. Point interstitial and dimer almost would have the same behavior except that a dimer needs a bigger space for accommodation. This mimic is also supported by Bader effective charge calculations: they almost have the same charge too (see below). However, this does not suggest the stability of oxygen dimers in UO_2 since point oxygen interstitial always has a lower per atom formation energy.

Our calculations also present a remarkable system size dependence in formation energy, which is in contrast to that of GGA results where values of -2.6 and -2.5 eV were obtained for $C1_1$ and $C2_1$ configurations (almost size independent), respectively,[13] revealing the limitation of applying the pure GGA to defects in spite of its impressive performance in energetics of perfect bulk UO_2.[2] No magnetic ordering and volume relaxation were considered in that GGA calculation.[13] A discrepancy about 1.2 eV with our result for $C1_1$, however, cannot be covered by these effects since volume relaxation would definitely increase the discrepancy, and magnetic contribution cannot be of that magnitude, and it should therefore be attributed to the behavior of localized $5f$ states.

The deepest formation energy shown in Fig. 2 is -2.32 eV (configuration $C4_2$) rather than the isolated approximation of a point interstitial's ($C8_1$) -2.17 eV. Actually, except those configurations with eight fluorite cubic cells, the defects in all other structures cannot be interpreted as isolated ones because the non-negligible interactions among their images arise from periodic conditions. This invalidates the defect stability analysis based on their formation energy directly. Mapping these configurations onto an alloy system can circumvent this difficulty, namely, to view these configurations
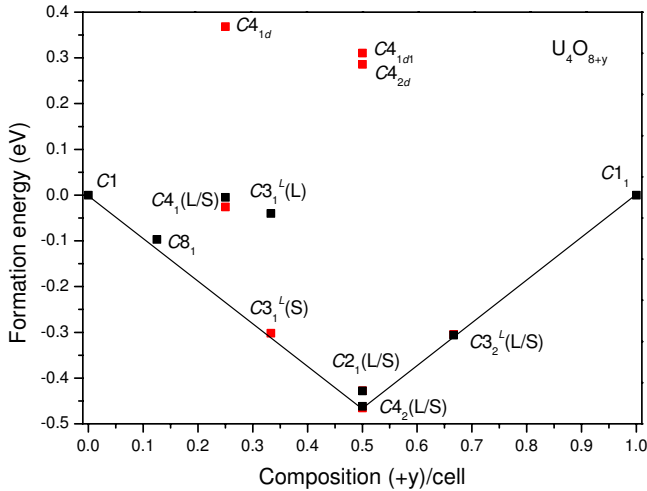
FIG. 3. (Color online) Relative formation energy of different phases in U_4O_{8+y}. $C8_1$ corresponds to an isolated defect approximation and other configurations must be interpreted as ordered defect phases.

(discard those with dimer) as an alloy system with oxygen interstitials distributing over the fluorite cubic centers (U_4O_{8+y}). Then, the extreme phases of this system are $C1$ and $C1_1$. Following this way, Fig. 2 transforms into Fig. 3 with the help of Eq. (2), where the solid line indicates the ground state hull. We then find that $C3_1^L(S)$ and $C3_2^L$ are close to be ground states, while $C8_1$, the isolated point interstitial approximation, will decompose into a mixture of $C1$ and $C4_2$ phases. This means that defect clustering is *inevitable* when $x \geq 0.03$.[39] Since $C4_2$ may not be the physical ground state (neutron diffraction experiments suggested that no octahedral site should be occupied around this composition[7,8]), this limit can be lowered further. On the other hand, it seems reasonable to assume that $C8_1$ has already approached the limit of an isolated point interstitial, namely, no notable formation energy would be gained or lost if enlarge the system to $C27_1$ or $C64_1$. If it is true, then the isolated point interstitial will always exist when $x \to 0$. Its site, according to structure symmetry, should be the octahedral position. It is worth noting that the PDM fails at about $x \sim 10^{-4}$ instead of 10^{-2} with GGA formation energies.[13] This 2 order discrepancy is due to the inaccuracy of the formation energies they used, which can be improved greatly by the LSDA+U method, see Sec. III G for details.

2. Other defects

Point oxygen vacancy and uranium defects are all modeled in a system with eight fluorite cubic cells, namely, by $C8_{-1}$ and $^uC8_{\pm1}$. The volume change in $C8_{-1}$ is in accord with that of point oxygen interstitials, linearly decreasing with an increased x, fitting to $\triangle V = 0.01 - 14.7x$, as shown by the solid line in Fig. 1. Uranium vacancy also obeys this law, whereas the interstitial has a much rapid change. Totally, they still decrease monotonically with x, but they are no longer linear. All three defects have a formation energy larger than 7 eV, which is in contrast to previous *ab initio*

results. We prefer to postpone this discussion to Sec. III G with Frenkel and Schottky defects together.

C. Charge transfers

It has long been believed that dissolving oxygen in UO_2 will *oxidize* U^{4+} to U^{5+}, even the U^{6+} state. The exact charge transfer induced by defects, however, is unclear. Qualitative analysis is accessible to this problem with empirical shell model[40]; nevertheless, the calculated energy sensitively depends on atomic positions,[41] obscuring its applicability to defects with noticeable structure deformations. A direct calculation of the charge state from first principles is therefore desired.

1. Oxygen interstitials

The calculated Bader effective charges using electronic density generated with the VASP code are listed in Table II, where the interstitials and the lattice oxygens that forming a dimer are excluded from the average operations and listed separately in the "defects" column. We find all oxygen interstitials that occupy the cubic body center having a charge state close to the lattice oxygens, especially in the $C8_1$ phase where the difference is only 0.03e. In $C8_1$, the disturbance to lattice oxygens is also small; the largest charge transfer is just 0.05e. A similar situation holds for uranium atoms, except that two of them lost about 0.24e, which directly contribute to the standard deviation. Considering that oxygen and uranium in perfect UO_2 only have charges of -1.28 and 2.56e, which are all smaller than the nominal chemical valences but close to that of a partially ionic model that widely used in semi-empirical potentials,[41,42] we can reinterpret the Bader charges by multiplying a scaling factor to make them comparable to the chemical valences. In this sense, the change of the charge state in these two uraniums should be about 0.5e, i.e., they are oxidized to $U^{4.5+}$ instead of U^{5+}. The transferred charges, however, cannot cover the amount absorbed by the interstitial oxygen, and all other normal uraniums and oxygens have also lost a small portion of their charge. This observation is in contrast to the conventional expectation and reveals the difficulty to oxidize uranium to a higher valence state. The charge transfers in other configurations also support this point: in all cases, each oxygen interstitial can oxidize *two* and only two uraniums to $U^{4.5+}$, while leaving others almost unchanged, no higher valence state of uranium has been observed. As to which uranium is apt to be oxidized, obviously the answer is the nearest neighbors (NNs) of the defect, but oxidization of some next NNs was also observed. It is worth pointing out that we did not find a sensitive dependence of the charge state on the Hubbard U parameter.

The more deformed the geometry is or, equivalently, the more interstitials the system contains, the charge state of lattice atoms are disturbed more drastically. It is clear by comparing the charge transfers in $C3_1^L$ with $C3_2^L$ or $C4_1$ with $C4_2$. The largest Δ_{max} for oxygen takes place in $C1_1$ with the largest composition, and in $C4_{2d}$ with a dimer. The smallest Δ_{max} for uranium and oxygen are in $C4_{1d}$, also containing a dimer, both are $-0.03e$. The difference between $C4_{1d}$ and

TABLE II. Bader effective charges of UO_2 with defects: average charge q, standard deviation σ, difference from that in perfect UO_2 δq, and the maximal transferred charge Δ_{max} (± 0.02). All are units of positron charge e.

Label	Defects q	Uranium				Oxygen			
		q	σ	δq	Δ_{max}	q	σ	δq	Δ_{max}
$C1$		2.56	0.0	0.0	0.0	−1.28	0.0	0.0	0.0
$C1_1$	−1.04	2.62	0.11	0.07	0.26	−1.18	0.004	0.10	0.11
$C2_1(L/S)$	−1.15	2.63	0.11	0.08	0.27	−1.24	0.02	0.03	0.07
$C4_1(L/S)$	−1.18/−1.14	2.60	0.08	0.04	0.25	−1.26	0.03	0.02	0.08
$C4_{1d}(S)$	−0.61(−0.77)[a]	2.56	0.02	0.01	−0.03	−1.28	0.01	0.0	−0.03
$C4_{2d}(S)$	−0.66, −0.59	2.60	0.08	0.04	0.26	−1.26	0.03	0.02	0.12
$C4_2(L/S)$	−1.19/−1.20	2.61/2.63	0.10	0.07	0.23/0.25	−1.24	0.02	0.04	0.07
$C8_1$	−1.24	2.58	0.05	0.03	0.24	−1.27	0.02	0.01	0.05
$C3_1^L(L/S)$	−1.16	2.60	0.09	0.04	0.25	−1.25	0.03	0.03	0.10/0.08
$C3_2^L(L/S)$	−1.10, −1.13	2.64	0.11	0.09	0.26/0.28	−1.23	0.02	0.05	0.09
$C8_{-1}$		2.53	0.09	−0.03	−0.34	−1.28	0.01	−0.00	−0.03
$^{u}C8_1$	1.61	2.51	0.09	−0.04	−0.25	−1.28	0.01	−0.00	−0.03
$^{u}C8_{-1}$		2.59	0.08	0.04	0.26	−1.26	0.03	0.02	0.13

[a]Value in the parentheses is for the atom sited on the oxygen sublattice.

$C4_{2d}$ is that the former contains only one interstitial that bonds to a lattice oxygen and the latter contains two interstitials that bond to each other. Table II illustrates that in the former case, no charge has been transferred from other lattice atoms, and only charge redistribution within the dimer is involved that makes it to have a total charge close to a lattice oxygen; in the latter case, however, absorbing charges from other atoms is necessary and gives them a similar charge state as the interstitial in $C4_1$; especially, here only two uraniums are oxidized to $U^{4.5+}$ state despite the fact there are two interstitials presented. The total charge of the dimer, $−1.25e$, close to a lattice oxygen in UO_2 indicates that it should actually be O_2^{2-}.

It is worth noting that oxygen changes its charge state almost continuously but it is *discrete* for uranium when its charge is lost. That is, except those atoms who lost $\sim 0.25e$, the changes of charge in other uraniums are less than $0.03e$. Moreover, the discrete loss of charge is always accompanied by lowering the local moment of uranium from $\sim 2\mu_B$ to $\sim 1\mu_B$. Since the local moment of uranium in UO_2 originates from localized $5f$ states, it is obvious that $5f$ electrons contribute to this process greatly. This can be understood in the partially ionic charge model: although the chemical valence of uranium in UO_2 is 4+, Table II shows that the physical valence only has 2.56+. Namely, only the $7s^2$ and a fraction of $6d^1$ electrons are completely transferred to oxygen. Uranium cation still holds about $0.24e$ of the $6d^1$ electron and the other remainder forms two weak U-O covalent bonds, each of which has a portion of $\sim 0.2e$. When oxidized by oxygen interstitials, the cation completely loses its $6d^1$ electron (transferred to the interstitial atoms). As a consequence, one of the localized $5f$ states becomes the outermost orbit, which spreads extensively, and the cation eventually loses half of its local moment. This mechanism also explains the difficulty to oxidize uranium to a higher charge state since transferring a $5f$ electron requires much larger energy than $6d$ one.

2. Other defects

In the point oxygen vacancy case (configuration $C8_{-1}$), the uranium cations gain charges and decrease the average valence to 2.53+, but the disturbance to retain oxygen is small. The largest charge transfer for uranium is $−0.34e$; associating with three other uranium atoms, each of them gets an extra charge of about $−0.25e$. Compared to the interstitial case, here no notable change in the local moment was observed. The value of $−0.34e$ implies that the cation has retracted the portion of electrons shared by the removed oxygen ($\sim 0.1e$) and $−0.25e$ indicates that each quarter-filled states of $6d$ electrons seems more stable than continuous occupancy.

Point uranium vacancy is analogous to two oxygen interstitials in which there are four uranium cations that lost their charge, three NNs and one next next NN, ranging from 0.23 to $0.26e$. All of them also lost half of their local moments. The change in other uraniums is negligible. However, it severely disturbs the oxygens, with a Δ_{max} as high as $0.13e$, even though the averaged charge is still close to the perfect one. The oxygen charge state in $^{u}C8_1$ is almost the same as in $C8_{-1}$, except that here there are six (NNs) instead four uraniums that gain charge, ranging from $−0.19$ to $−0.25e$. Again, there is no apparent impact on other atoms. The extra charge provided by the interstitial uranium is almost completely absorbed by its six NNs. The magnetic ordering has been severely damaged, and the change in exchange interaction made some $5f$ electrons flip their spins, but no uranium was observed to have a moment of $\sim 1\mu_B$.

D. Oxygen dimer in UO_2

As previously mentioned, although oxygen dimer has a similar behavior in energetics and charge state as a single oxygen interstitial, it is actually an ionic molecule and it forms when oxygens are forced to be close to each other.
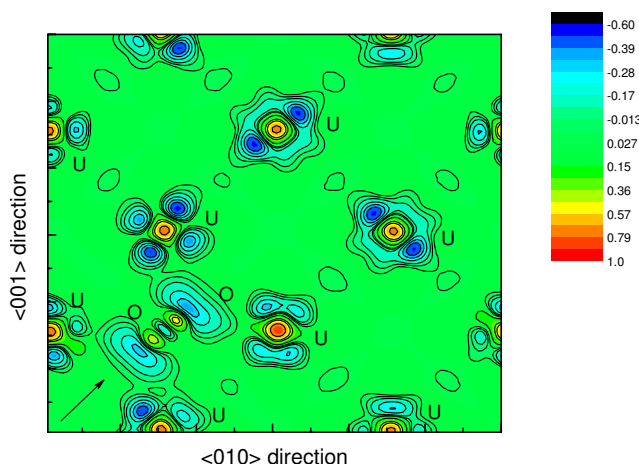
FIG. 4. (Color online) The difference charge density of an oxygen dimer in $C4_{2d}$ configuration projected onto the [100] plane crossing the dimer center. An analogous density holds for the dimer in $C4_{1d}$.

However, this is difficult due to the energy barrier between the individual atoms. In UO$_2$, irradiation provides enough excess energy to overcome this barrier. For example, in an α decay the recoil of the daughter nucleus produces a ballistic shock with an energy release of about 70 keV,[43,44] which frequently takes place in nuclear fuels. Nonetheless, this cannot survive the dimers to equilibrium conditions even if they transiently appear. Another situation where oxygen dimers can be observed is near the *surfaces* exposed to oxygen gas. Oxygen molecules adsorbed onto the UO$_2$ surface will obtain additional charges and then will diffuse inward. Decomposing the molecule at the vacuum side of the surface is almost impossible due to the large binding energy, while in UO$_2$ side it prefers the oxygen sublattice sites instead of the interstitial positions, where it decomposes into individual interstitials, with a barrier only about 0.21 eV (see below).[45]

Figure 4 shows the difference charge density (reference to the corresponding atomic charge) of an oxygen dimer in UO$_2$ ($C4_{2d}$) projected to the [100] plane, which is indicated by the arrow. The covalent bond between two interstitial oxygens is evidently present. A similar picture has been observed in $C4_{1d}$ configuration or a natural O$_2$ molecule. Analysis shows that it is, in fact, an O$_2^{2-}$, with the two additional electrons occupying the $2p\pi^*$ antibonding orbitals, and the final bond order is 1. The calculated bond length is 1.39 Å, which is slightly shorter than the experimental value of 1.49 Å.[35] This discrepancy is due to the compression from the oxygen cage and can be removed. For example, when the dimer is formed by bonding to one lattice oxygen ($C4_{1d}$), where the charge state is still similar ($-1.38e$), the bond length extends to 1.47 Å, which is in good agreement with experimental data.

Accomodating the oxygen dimer in UO$_2$ leads to a swelling of the system volume (see Table I). The induced stress forces them to orient in the $\langle 111 \rangle$ direction and to occupy the Willis O$''$ sites. In energetics, the oxygen dimer in UO$_2$ is metastable, (see Fig. 2). Its decomposition process can be modeled by successively moving the interstitial oxygen (as a test atom) in $C4_{1d}$ along the $\langle 111 \rangle$ direction until the cubic center, which is the most possible separate path. The resulted potential shape is shown in Fig. 5, where δd is the initial distance between the two oxygens and Δd is the final (dimer) length. The *structure frozen* line was obtained by fixing the cell and all other atomic positions, whereas the *optimized* one was resulted from a full relaxation of the cell volume and shape and the nearby atomic coordinates surrounding the defect.

Note that a distance of $\delta d = 2.2$ Å represents the state where the initial position of the test oxygen is already close to the cubic center. From Fig. 5, we get that the critical distance to break a dimer is about 1.73 Å with a barrier of 0.21 eV. The inset gives the variations of system volume and (negative) Bader atomic charges of the two oxygens, demonstrating a drastic behavior around the breaking point. Two points need to be noticed here: the large charge transfers and the contraction of system volume. The latter confirms that the atomic size effect is not an important factor for oxygen interstitials in UO$_2$ where chemical interaction is over-

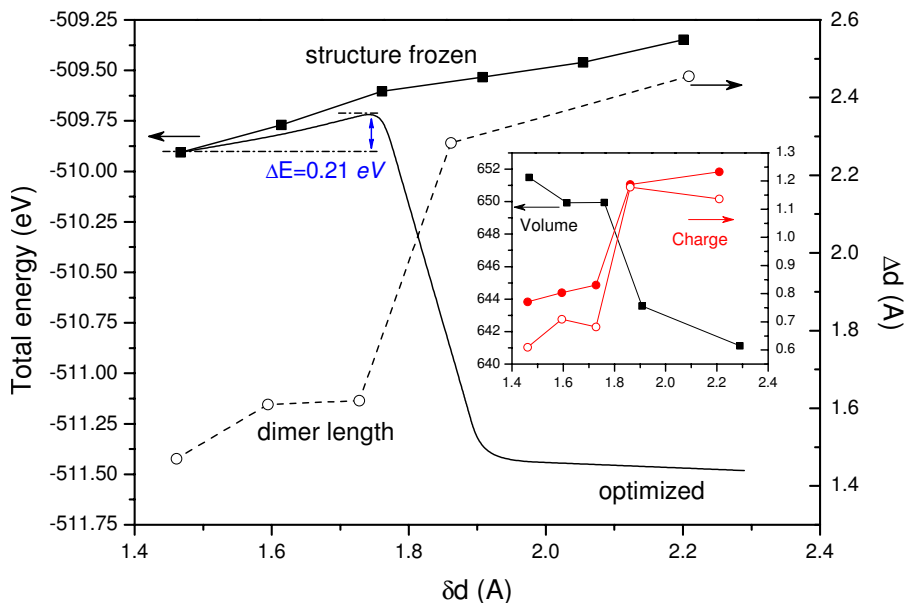

FIG. 5. (Color online) Behavior of oxygens during a dimer decomposing process along $\langle 111 \rangle$: potential shape (solid lines) and equilibrium intradistance (dashed line). δd is the initial separate distance and Δd is the final bond length. Inset: Changes in cell volume (black line) and atomic charges (red lines).

whelming. A deduction of this is that a single oxygen interstitial can occupy a site other than the cubic center despite the fact that it has the largest space. Indeed, no experiment has detected the occupation of this site in UO_{2+x} when $x \geqslant 0.1$. Chemical interaction might prefer other sites if volume is expanded. As the "structure frozen" line shows, interstitial oxygen is apt to forming dimers when the volume is fixed at 651.49 Å^3. Therefore, oxygen dimers may also exist at regions with negative stresses.

As the limit case of an interstitialcy diffusion model, forming an oxygen dimer in UO_2 requires an energy of ~ 1.75 eV (Fig. 5), which is compatible to the NEB migration energy of 1.1 eV.[16] This magnitude of migration energy corresponds to $\delta d \simeq 1.8$ Å, with an equilibrium intra-atomic distance of about 2.0 Å and atomic charges of $\sim -1.0e$. Therefore, a charge oscillation induced by oxygen diffusion is about $0.2e$, which is almost the same level in oxidizing one uranium.

E. Vibrational frequencies

Raman and infrared spectroscopies provide information about atomic vibrations. These techniques can be employed to detect defect clusters by searching the characteristic vibrational frequencies. At finite temperatures, these frequencies directly contribute to the formation energy and structural thermodynamic stability.

Vibrational frequencies of single oxygen interstitial (has three modes) and dimer (has six modes) in $C2_1$, $C4_1$, $C4_{1d}$, and $C4_{2d}$ configurations were calculated. In all calculations, we aligned the magnetic ordering direction along the shortest axis (S), which always has the lowest energy. Only harmonic frequencies were computed here and have omitted all anharmonic effects. For fluorite UO_2, we have checked that the contribution from the latter is very small for oxygen and uranium interstitials (within ± 3 cm^{-1}). Table III lists the calculated frequencies (ω), as well as the equilibrium bond length for dimers (d_0) and formation energies (ΔE). Due to the compression from the oxygen cage, the vibrational frequencies in $C4_{2d}$ have greater value than their counterparts in $C4_{1d}$. The stretch model of O_2 molecule (with the largest ω) has been greatly softened when incorporated in UO_2. This is analogous to the incorporation of H_2 in an interstitial position of semiconductors,[46] where a decrease of the binding energy, an increase in the bond length, and a lowering of the vibrational frequency were observed. The underlying physics, however, might be different. In this case, by comparing the calculated Bader effective charges with the partially ionic model of UO_2,[42] we can identify that the nominal charge of the oxygen dimers should be about $-2.0e$. The variation of bond length confirms this interpretation. Consequently, the frequency of the stretch model is lowered from 1588.6 to 995.4 cm^{-1} in $C4_{2d}$ and 795.4 cm^{-1} in $C4_{1d}$.

According to the calculated static energies, $C4_{2d}$ will decay to $C2_1$ and $C4_{1d}$ will eventually decay to $C4_1$ (see $\triangle E$ in Table III). Computed frequencies indicate that thermal vibrations would accelerate this process further. Figure 6 gives the difference of free energy between $C4_{2d}$ (F_d), $C2_1$ (F_s), $C4_{1d}$ (f_d), and $C4_1$ (f_s) calculated with their formation energies

TABLE III. First principles results for structural, energetic, and vibrational properties of oxygen interstitial and O_2 dimer in different configurations. For comparison, calculated values for O_2 in vacuum are also listed. ΔE is the energy difference between interstitial O/O_2 and vacuum O_2 (formation energy per pair interstitials), d_0 is the equilibrium bond length, q is the Bader effective charge, and ω is the harmonic frequency. Note that the q in the last row is just to label the experimental condition.

Label	ΔE (eV)	d_0 (Å)	q (e)	ω (cm^{-1})
$C2_1$	-4.496		-1.15	292.5, 316.7, 403.9
$C4_1$	-2.993		-1.14	373.3, 386.6, 397.5
$C4_{1d}$	0.159	1.47	$-0.61(-0.77)$	273.6, 345.3, 353.9
				452.8, 473.6, 795.4
$C4_{2d}$	-1.642	1.39	$-0.66, -0.59$	447.4, 482.3, 496.6
				608.5, 637.2, 995.4
Vacuum	0	1.22	0.0	1588.6
Expt.		$1.21/1.49^a$	$0.0/-2.0$	$1580.2^b/$

^{a}Reference 35.
^{b}Reference 34.

(Table I) and vibrational frequencies (Table III), respectively. The rapid drop of the free energy differences with increased temperature implies that metastable oxygen dimers in UO_2 have a very short lifetime at finite temperatures and with little possibility to occupy the cubic center sites: they must have been decomposed before entering the oxygen cage.

F. Defect clustering in UO_{2+x}

This section is devoted to the possible defect *clustering pattern* in UO_{2+x}. Instead of directly computing the formation energies, here, we focus on the *local stability* of O′ and O″ sites in different circumstances. This method cannot determine what cluster is the most stable one, but it *does* rule
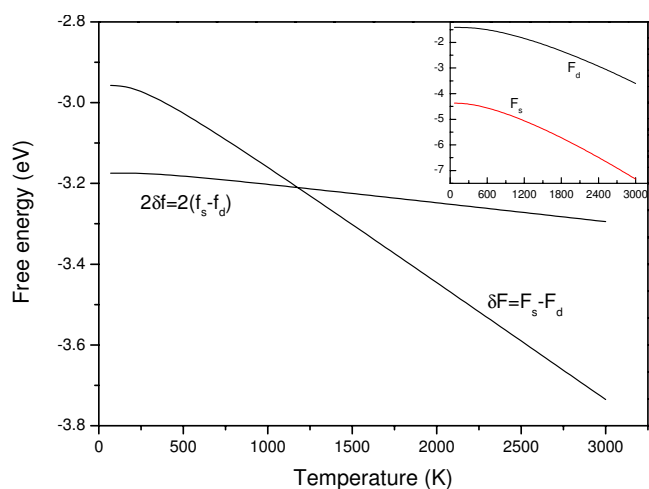

FIG. 6. (Color online) Variation of free energy difference contributed from interstitial vibrations. Inset: the free energies of a dimer in $C4_{2d}$ and its relative stable state $C2_1$ as a function of temperatures.
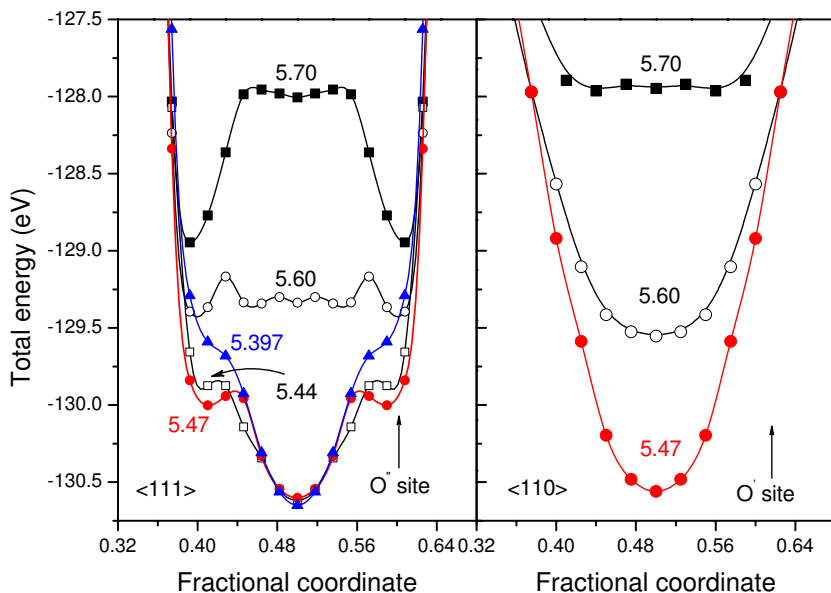
FIG. 7. (Color online) Potentials for an oxygen interstitial in UO$_2$ along the $\langle 111 \rangle$ (left) and $\langle 110 \rangle$ (right) directions crossing the cubic center. The numerics refer to the lattice constant and arrows point to the position of the O$'$ or O$''$ site. Fractional coordinate 0.5 denotes the cubic center.

out some combinations of O$'$, O$''$, and oxygen vacancies.

For this purpose, we calculated the potential landscape felt by a test oxygen atom. Just one fluorite cubic unit cell was used. Here, since the cell and all atomic coordinates have been frozen up except that of the test oxygen, the error introduced by periodic conditions is in proportion to the second order of the charge density variation $\delta \rho$ that is induced by images of the test atom. This precision is enough for a qualitative analysis (ionic interactions among the test atom's images contribute only a constant to the energy and are therefore irrelevant to the problem).

1. Local stability of basic clustering modes

At first, we check the local stability of a single O$'$ and O$''$ site. Figure 7 shows the potential shapes crossing these two sites. It is seen that the O$''$ site becomes metastable when the lattice constant increases to about $a = 5.44$ Å. Moreover, isotropic expansion stabilizes this site further, which makes it the global minimum if $a \geq 5.6$ Å. A single O$''$ interstitial actually forms a dimer with the nearest lattice oxygen and this behavior is in consistence with the structure frozen curve in Fig. 5. However, this effect does not benefit the stabilization of the O$'$ site. Under ambient conditions, the experimental lattice constant for UO$_{2+x}$ is within 5.45–5.47 Å; therefore, a single O$'$ or O$''$ oxygen interstitial (as well as clusters formed by them only) is almost unstable.

The simplest cluster involving one oxygen vacancy, say, a V-O$'$ or V-O$''$ pair, is obviously unstable since nothing can prevent them from annihilating. The next triple cluster is the V-O$'$(O$''$) pair stabilized by an O$'$ or O$''$ interstitial. Considering the short distance between the nearest O$'$ and O$''$ sites, the situation should be quite similar for them. Therefore, hereinafter we only consider the cases that are incorporated with V-O$'$ pairs. The potential shape for an O$'$(O$''$)-V-O$'$ cluster was calculated in an analogous manner except that a lattice oxygen (0.75,0.75,0.75) was moved to (0.883, 0.5, 0.883), which is the nearest O$'$ site, to create the V-O$'$ pair, as shown in Fig. 8. Although the curve along $\langle 110 \rangle$ already

changes asymmetrically about the cubic center (with a fractional coordinate of 0.5), O$'$ is locally unstable since it will decay to O$''$ (with a swallow trap), then finally to a position beyond the (0.75,0.75,0.75) site. This rules out the O$'$-V-O$'$ (V-2O$'$) and O$''$-V-O$''$ (V-2O$''$) triple clusters that distribute symmetrically about a lateral of the oxygen cage.

To locally stabilize the O$'$ site, we have tried all possible combinations and find that two nearest oxygen vacancies seem necessary. Figure 9 gives the potentials that is incorporated with two V-O$'$ pairs. These O$'$ sites should be in otherwise empty oxygen cubes that do not share the lateral linking the two vacancies with the original one. The pairs are thus created by moving (0.75,0.75,0.75) oxygen to (0.617,1.0,0.883) and (0.75,0.75,0.25) to (1.0,0.617,0.117), respectively. We see that it prefers the O$'$ but not the O$''$ site. In fact, this cluster would become the Willis 1:2:2 (O$'$:V:O$''$) cluster[7] if the two O$'$ interstitials move to their nearest O$''$ sites and form two V-O$''$ pairs rather than the V-O$'$ ones. Figure 9 shows that it might be locally stable, which is in consistence with empirical calculations.[40] The stabilization of O$''$ by V-O$'$ pairs sited in the otherwise empty oxygen cages is unclear in Fig. 8, but calculations show that a V-2O$'$ triple locally stabilizes O$''$ (O$''$-V-2O$'$) as well as a V-2O$''$ triple (O$''$-V-2O$''$).

Thus, we finally arrive at the conclusions that (i) O$'$ or O$''$ interstitials cannot exist by themselves and (ii) each O$'$ site must be incorporated with two nearest oxygen vacancies, while O$''$ can be stabilized by a V-2O$'$(O$''$) triple. This means that the possible clustering pattern for oxygen defects should only be (a) V-3O$''$ or V-4O$''$ isolated clusters, which is in the same manner of split interstitial where several atoms share a single lattice site, and (b) cluster chains of V-O$'$-V or V-2O$'$-V by sharing the vacancy sites. These chains should be closed to have all O$'$ interstitials locally stable while minimizing the vacancy-interstitial ratio: (c) cluster of V-(2)O$'$-V chains terminated by two V-(2)O$''$ clusters at both of the extreme sides by sharing the vacancy sites. We call these small fractal clusters the *Willis-type* cluster, including 1:2:2,[7] 2:2:2,[8,10] 4:3:2 clusters,[40,47] and so on. However, their
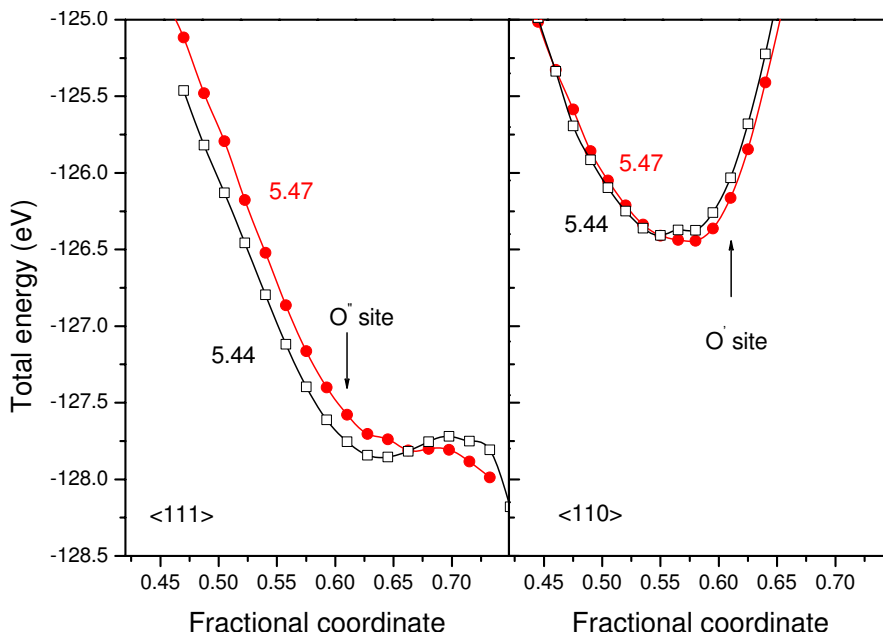
FIG. 8. (Color online) Potentials for an oxygen interstitial in UO_2 (incorporated with a V-O' pair) along the $\langle 111 \rangle$ (left) and $\langle 110 \rangle$ (right) directions crossing the cubic center (fractional coordinate 0.5).

actual stability is still unknown, which requires accurate knowledge about their formation free energies.

2. Phase diagram for clusters

In UO_{2+x}, the positive formation energy of oxygen Frenkel pair and the small energy gain from interactions among interstitials (see Fig. 2) imply that the only way to reduce the energy increment from creating vacancies is via vacancy-interstitial (V-I) interactions. Obviously, the nearest V-I pairs contribute the most. Therefore, the relative stability of clusters can be judged roughly by counting the number of nearest interstitials around each vacancy. For example, in a 1:2:2 cluster, each vacancy only has 2 V-I pairs, while in 2:2:2 it has 3, and in 4:3:2 it has 3.3. This means that 1:2:2 should be metastable, even though it can explain the concentrations measured by Willis in 1964.[7] However, these data can also

be explained by a larger cluster with four O'' interstitials, namely, a 2:2:4 cluster where each vacancy has four V-I pairs. Willis-type clusters are necessary in order to explain the large concentration of O'' interstitials, which is impossible by only using cuboctahedral cluster [belonging to pattern (b)]. For example, the data for crystal A by Murray and Willis[48] obviously belong to 2:2:2 clusters, while crystal B should be a mixture of 4:3:2 and cuboctahedral clusters or a 6:4:2 cluster.

However, a big Willis-type cluster is unfavorable since the disturbance to fluorite lattice is in linear proportion to its size. A similar situation holds for a loosely closed chain of pattern (b). In this sense, the most regular and close-packed defect cluster, the cuboctahedral cluster, takes the advantage of sharing the space with all vacancies and interstitials to minimize the damage to the matrix. Also, one fluorite cubic

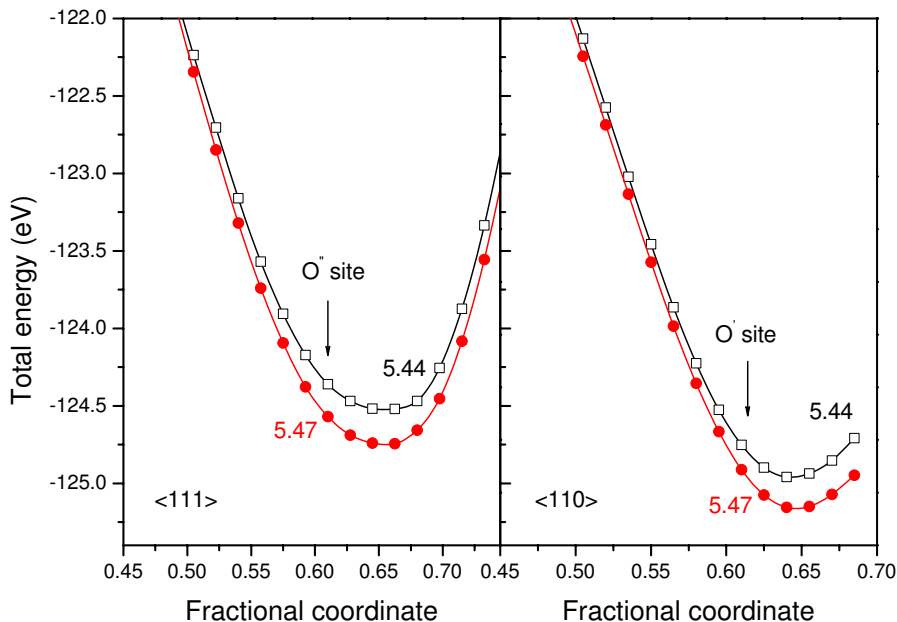FIG. 9. (Color online) Potentials for an oxygen interstitial in UO_2 (incorporated with two V-O' pairs) along the $\langle 111 \rangle$ (left) and $\langle 110 \rangle$ (right) directions crossing the cubic center (fractional coordinate 0.5).
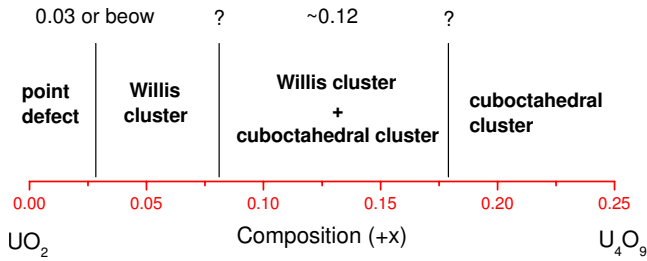
FIG. 10. (Color online) A schematic *phase diagram* for oxygen defect clustering in UO_{2+x}. The boundaries, however, are not clearly known.

cell can accommodate one (or less) Willis-type cluster or one cuboctahedral cluster. However the former provides only two excess anions, while the latter provides five excess anions. When composition x increased, cuboctahedral cluster has a big advantage over the Willis-type cluster, not to mention that each of its vacancy has a number of V-I pairs greater than 3. As for the clustering pattern (a), though there are three (V-$3O''$) or four (V-$4O''$) V-I pairs for each vacancy, we can discard them at first since no experiments showed so high concentration for O'' interstitials.

It becomes evident when the variation of O' : O'' ratio is checked as x increased: around $x = 0.11-0.13$, three different data sets were observed [0.08:0.16,[7] 0.14:0.12, and 0.33:0.10 (Ref. 48)], implying the occurrence of Willis-type clusters. As x approaches 0.25, however, this ratio drastically increases[4,5,49] and shows the dominance of cuboctahedral clusters. Therefore, by taking the stability of point interstitial at low x into account, one concludes that there is a quasi-phase-diagram for oxygen clusters in UO_{2+x}, as shown in Fig. 10.[50] Determining the exact geometry of ground clusters and their boundaries would be the center of future works in this field.

It is worth pointing out that such kind of defect clustering is not unique to uranium dioxide. According to the formation energy of point defects, one can classify binary compounds into three classes: (A) all formation energies are positive, (B) only one of the formation energies is negative, and (C) both cation interstitial (vacancy) and anion vacancy (interstitial) have negative formation energies. There is no off-stoichiometry driven force in case (A) and it disfavors extensive defect clustering. However, the negative formation energies in the other two cases will drive the system to a nonstoichiometric composition where defect clustering becomes favorable. This is because the interaction among defects can lower the system energy greatly and lead to a pure defect clustering (via a full vacancy-interstitial annihilation) or mixed defect clusters that contain both vacancy and interstitial. Also, the mixed cluster is possible only when the point defect with positive formation energy (vacancy or interstitial) has the function to stabilize the other defects in an energy favorable configuration (in a similar concept of the split-interstitial defect mechanism). Obviously, UO_2 fulfills these conditions (see Fig. 2 and previous subsection) and belongs to case (B), where oxygen interstitial has a negative formation energy and clustering involves no uranium sites. On the other hand, case (C) contains clusters composed of both cation and anion defects, and might exhibit more complex behaviors.

G. Concentration of defects

1. Generalization of the PDM

The PDM was introduced by Matzke[14] and Lidiard[15] to analyze the populations of defects in UO_{2+x}, where x indicates the deviation from stoichiometry. This model is based on the hypothesis that the defects responsible for the deviation from stoichiometry in UO_{2+x} are isolated point defects. However, it has been known for long that oxygen interstitials form clusters and PDM usually performs poorly even at small $|x|$.[12,13] Therefore, it is worth generalizing this model beyond the point approximation. Since defect concentrations are traditionally defined in a lattice model as the number of defects present divided by the number of available sites for the defect under consideration, the most general and elegant generalization of PDM would be the cluster variation method (CVM),[51] which is also based on the lattice gas model and computes cluster configurational entropy explicitly. The related effective cluster interactions can be determined by the cluster expansion method (CEM).[52] For UO_{2+x}, at first sight it seems to be a quaternary system (V_O, V_U, I_O, and I_U) and cannot be tackled by modern CVM and CEM techniques. However, since defects on the uranium subsystem are usually isolated point defects that couple with oxygen subsystem via Schottky defects, in fact, only oxygen defects need to be treated explicitly. However, in order to include O' and O'' sites in the calculation, one has to use an extended lattice, which introduces another two difficulties.

The first one relates to the local stability of O' and O'' sites since these sites are not well defined and usually a full relaxation is required to get the optimized geometry. However, in most configurations they are not at the potential minima and makes it impossible to include the relaxation effects in the *ab initio* CEM procedure. Fortunately, an algorithm proposed by Geng *et al.*[53] can simply tackle this problem. The second difficulty is that most configurations on the extended oxygen sublattice is unphysical, i.e., some distances among oxygen sites are too short to be allowed. To exclude these unphysical configurations, one has to use *loose clusters* to expand the energy, which drastically deteriorates the convergence of cluster expansion.

If all non-negligible clusters are independent and uncorrelated, a simple approximation exists to calculate cluster populations. Two clusters are called independent if none of them is the other one's subcluster (or loosely cannot dissociate or combine into other clusters). This ensures that all cluster concentrations are completely independent. Assume that there are M such kind of clusters under consideration, then the system free energy can be written as

$$F = \sum_{i=1}^{M} \rho_i (E_i + \kappa_B T \ln \rho_i) \qquad (5)$$

in the closed regime (in which the system cannot exchange atoms with the exterior). Here, E_i stands for the ith cluster's formation energy. Minimizing this free energy with respect

to each cluster density ρ_i (under the condition that x is fixed) gives

$$\rho_i = g_i \exp\left(\frac{-E_i}{\kappa_B T}\right), \tag{6}$$

associated with the composition equation

$$x = f(\rho_1, \ldots, \rho_M). \tag{7}$$

In Eq. (6), the factor g_i is introduced to account for the degeneracy if the cluster has internal freedom, while nondegenerated states can be treated as independent. This gives the internal entropy contributions and is the most significant difference between the independent cluster approximation and PDM.

The PDM equations can be derived by considering only isolated point defect excitations (without internal structure): V_O, V_U, I_O, and I_U. In a closed system, the particle numbers must be conserved, which reduces the number of independent defect modes to 3. On the other hand, the formation energy reference state for point oxygen and uranium defects are usually different; therefore, one should instead use three independent combinations of these isolated defects to eliminate this ambiguity. The simplest candidates are oxygen and uranium Frenkel pairs and Schottky defect (or, equivalently, anti-Schottky defect). Consequently, $M=3$ and $i=1,\ldots,3$ correspond to the isolated Frenkel pairs and Schottky defect, respectively. In this way, Eq. (6) becomes

$$\rho_{FP_O} = \exp\left(\frac{-E_{FP_O}}{\kappa_B T}\right) \equiv [V_O][I_O], \tag{8}$$

$$\rho_{FP_U} = \exp\left(\frac{-E_{FP_U}}{\kappa_B T}\right) \equiv [V_U][I_U], \tag{9}$$

$$\rho_S = \exp\left(\frac{-E_S}{\kappa_B T}\right) \equiv [V_O]^2[V_U], \tag{10}$$

and the composition equation expressed in point defect populations

$$x = 2([V_U] - [I_U]) + [I_O] - 2[V_O]. \tag{11}$$

Equations (8)–(11) exactly comprise the PDM equations

To include cluster effects, taking $C4_2$ configuration as an example, we need to reinterpret the two interstitials as an *isolated* diagonal pair (dp). Assuming that this interstitial pair is predominant over the point one, then Eq. (8) is replaced by

$$\rho_{dp}[V_O]^2 = \exp\left(\frac{-E_{dp} - 2E_{V_O}}{\kappa_B T}\right), \tag{12}$$

where two isolated oxygen vacancies have been introduced to eliminate the ambiguity in extrinsic defect formation energy. Also, the composition equation becomes

$$x = 2([V_U] - [I_U]) + \rho_{dp} - 2[V_O], \tag{13}$$

where Eqs. (9) and (10) are kept unchanged. This procedure can be extended to easily include other independent clusters.

2. Defect concentrations in PDM

In the point defect approximation, the formation energy of a Frenkel pair of the X species is given by

$$E_{FP_X} = E_{V_X}^{N-1} + E_{I_X}^{N+1} - 2E^N, \tag{14}$$

and for the Schottky defect (S), it is given by

$$E_S = E_{V_U}^{N-1} + 2E_{V_O}^{N-1} - 3\frac{N-1}{N}E^N, \tag{15}$$

where N is the number of atoms and E^N is the total (or cohesive) energy in the defect-free supercell; $E_{V_X,I_X}^{N\pm1}$ is the energy of the cell with the defect. Here, we use $C8_{\pm1}$ and $^uC8_{\pm1}$ to model the point defects; thus, $N=96$ and E^N and $E_{V_X,I_X}^{N\pm1}$ can be obtained by timing 8 to the corresponding cohesive energies listed in Table I.

The formation energies of the defects obtained are listed in Table IV. They are compared to the previous theoretical results[11–13,37,54] and PDM estimates based on diffusion measurements.[14] Note that the GGA+U employed the same U parameter as in this work. A detailed comparison of its results with LSDA+U can be found in Ref. 2. Despite the fact that it produced a similar band gap and local magnetic moment as LSDA+U, it predicted a *big* lattice constant of $\sim$5.55 Å. In Fig. 7, we know that this would lead to an underestimation of the oxygen interaction with the matrix. Table IV proves this by showing a smaller absolute value of the oxygen interstitial and vacancy formation energies than any other calculations. However, this failure is not from GGA but the parameter of U.[55] Besides, this U also greatly underestimates the formation energy of uranium interstitial, implying that one needs to fit an own U value for GGA functional separately.

The improvement of LSDA+U over the pure GGA or LDA results is significant. Both the latter underestimate the formation energy of uranium vacancy by about two times and 10%–20% for oxygen vacancy. By the lump, LSDA+U corrects the energy by 50% and 38% for O-FP (Frenkel pair), 46% and 61% for U-FP, 89% and 83% for Schottky defects over GGA and LDA, respectively. This correctness makes our LSDA+U results the *ab initio* defect formation energies that *predict* the predominance of oxygen defects within a broad enough stoichiometric range over uranium ones (for the performances of LDA or GGA formation energies and the PDM anticipation, please see Refs. 12 and 13).

The defect concentrations or, equivalently, populations calculated with PDM equations are shown in Fig. 11. An arbitrary temperature of 1700 K is chosen. We see that oxygen interstitial dominates when $x>0$, while oxygen vacancy dominates when $x<0$. At $x\sim0$, O-FP overwhelms. This picture is in good agreement with diffusion measurements *interpreted* by PDM,[14] but different from neutron diffraction data where non-negligible oxygen vacancies were observed when $x>0$.[4–8,48] The population of oxygen vacancy predicted by PDM is too low to be true. To increase this population in the $x>0$ regime, one needs to take clustering effect into account.

TABLE IV. Formation energies (eV) of point defects in UO$_2$: uranium and oxygen vacancies (U-Vac and O-Vac), uranium and oxygen interstitials (U-Int and O-Int), Frenkel pairs (O-FP and U-FP), and Schottky defect (S).

	U-Vac	O-Vac	U-Int	O-Int	O-FP	U-FP	S
LSDA+U[a]	9.1	7.5	8.2	−2.2	5.4	17.2	10.6
GGA+U[b]	8.4	4.5	4.7	−0.4	4.0	13.1	5.8
GGA[c]	4.8	6.1	7.0	−2.5	3.6	11.8	5.6
GGA[d]	5.1	6.1	7.5	−2.6	3.5	12.6	6.0
LDA[e]	3.3	6.7	7.3	−2.9	3.9	10.7	5.8
LDA-LMTO[f]	19.1	10.0	11.5	−3.3	6.7	30.6	17.1
Semi-empirical[g]	80.2	16.9	−60.8	−12.1	4.8	19.4	11.3
PDM estimates[h]					3.0–5.8	9.5	6.0–7.0

[a]With eight fluorite cubic cells (this work).
[b]With eight fluorite cubic cells (Ref. 37).
[c]With two fluorite cubic cells (Ref. 13).
[d]With one fluorite cubic cell (Ref. 13).
[e]With two fluorite cubic cells (Ref. 12).
[f]Reference 11.
[g]Reference 54.
[h]Reference 14.

3. Defect concentrations with independent clusters approximation

By assuming that the oxygen diagonal pair in $C4_2$ is dominant over the single interstitial, one can formally calculate the clustering effect. It is not a promising assumption due to the small energy difference between them, while it can be used to analyze the influence of *pure* interstitial clusters that occupied only the octahedral sites on the vacancy populations (they should have similar effects). Also, it serves to show how the independent cluster approximation works out.

Using the defect formation energy of $C4_2$ and Eqs. (9), (10), (12), and (13), we calculated the defect populations following the same manner as PDM; the result is presented in Fig. 12. Here, note that ρ_{pd} turns out to have the same numerical value as $[I_O]$. We see that this pure clustering mechanism decreases the oxygen interstitial population, but that of oxygen vacancy in the $x > 0$ regime is still too low. Another problem raised here is that the population of uranium vacancy is closely pinned to that of the oxygen interstitial. It is not what we wanted. Roughly, Fig. 12 suggests that clusters associated with oxygen *vacancies* are necessary in order to greatly enhance the latter's concentration in the $x > 0$ regime and to pin that of the oxygen interstitial, as implied by the neutron diffraction measurements.
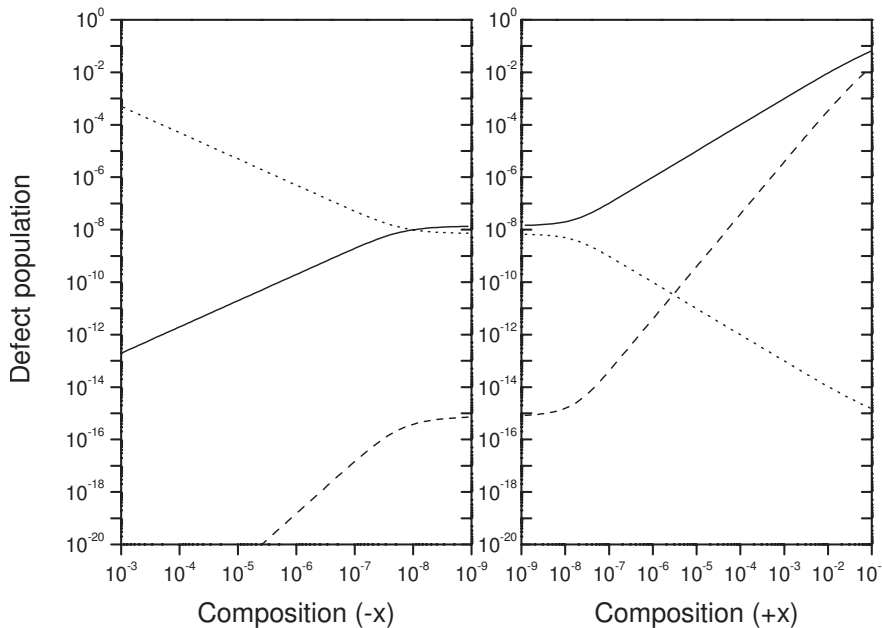

FIG. 11. Analysis of the point defect model at a temperature of 1700 K. Variation of the concentrations of point defects with the deviation from stoichiometry x: hypostoichiometric regime (on the left) and hyperstoichiometric regime (on the right). Solid (dotted and dashed) line indicates the concentration in oxygen interstitial (oxygen vacancy and uranium vacancy). The concentration of uranium interstitial is negligible.
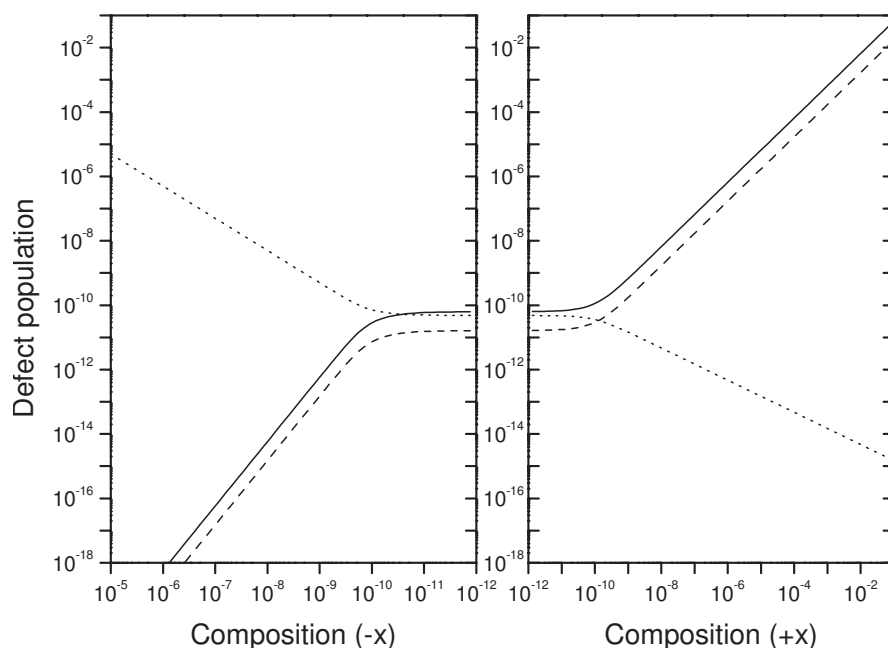
FIG. 12. Analysis of independent cluster model with isolated diagonal oxygen interstitial pair approximation. Others are the same as in Fig. 11.

IV. CONCLUSION

In summary, we performed a comprehensive calculation on defect properties in $UO_{2\pm x}$ with the LSDA+U method. The volume changes induced by defects and their formation energies were accurately computed. Analysis of these energies for a series configurations concluded that defect clustering is unavoidable when $x \gtrsim 0.03$, which is compatible to the experimental fact. Atomic charge calculations in Bader's definition, however, showed the difficulty to oxidize uranium to U^{6+} and the charged oxygen is apt to losing its electrons against common expectation. As the simplest interstitial cluster, oxygen dimer behaves in a manner similar to a normal oxygen in energetics and charge state. It was identified as ionic dioxygen molecule with two excess electrons. Static and vibrational free energy calculations, however, showed that it is quite unstable and might only be a transient state during oxidization process.

Oxygen dimer is the extreme case for interstitialcy diffusion of oxygen, which may induce a charge fluctuation with a magnitude less than $0.2e$. It also presents as a special case for Willis O'' site occupancy under stretch. The stabilization mechanism for this site under ambient conditions, however, is attributed to a V-$2O''(O')$ triple by the local stability analysis. Also, the O' site is stabilized only by the nearest oxygen vacancy pair. This comprises the basic clustering pattern for defects in UO_{2+x}: play with the four building blocks [V-$(2)O''$ and V-$(2)O'$-V] by sharing the vacancy sites. The actual stability of clusters should be judged by the formation energies, which is beyond the scope of this paper and, hence will be discussed in a future work. A quasi-phase-diagram for defect clusters vs composition was also proposed to explain the observed population ratios of O' and O'' sites, which, of course, requires further refinement step by step when more calculations and experimental data are available.

The formation energy of Frenkel pairs and Schottky defect calculated with LSDA+U have been improved more than 50% over the GGA and LDA results. With these energies and the point defect model, we showed the predominance of oxygen defects by first principles. Finally, we generalized the PDM to independent cluster approximation that allows us to compute the population of clusters and revealed the necessity to move on to Willis-type clusters.

[1] M. Idiri, T. Le Bihan, S. Heathman, and J. Rebizant, Phys. Rev. B **70**, 014113 (2004).

[2] H. Y. Geng, Y. Chen, Y. Kaneta, and M. Kinoshita, Phys. Rev. B **75**, 054111 (2007).

[3] J. Hering and P. Perio, Bull. Soc. Chim. Fr. **19**, 351 (1952).

[4] D. J. M. Bevan, I. E. Grey, and B. T. M. Willis, J. Solid State Chem. **61**, 1 (1986).

[5] R. I. Cooper and B. T. M. Willis, Acta Crystallogr., Sect. A: Found. Crystallogr. **A60**, 322 (2004).

[6] B. T. M. Willis, J. Phys. (France) **25**, 431 (1964).

[7] B. T. M. Willis, Proc. Br. Ceram. Soc. **1**, 9 (1964).

[8] B. T. M. Willis, Acta Crystallogr., Sect. A: Cryst. Phys., Diffr., Theor. Gen. Crystallogr. **A34**, 88 (1978).

[9] C. R. A. Catlow, in *Nonstoichiometric Oxides*, edited by O. T.

Sørensen (Academic, New York, 1981).

[10] G. C. Allen, P. A. Tempest, and J. W. Tyler, Nature (London) **295**, 7 (1982).

[11] T. Petit, C. Lemaignan, F. Jollet, B. Bigot, and A. Pasturel, Philos. Mag. B **77**, 779 (1998).

[12] J. P. Crocombette, F. Jollet, T. N. Le, and T. Petit, Phys. Rev. B **64**, 104107 (2001).

[13] M. Freyss, T. Petit, and J. P. Crocombette, J. Nucl. Mater. **347**, 44 (2005).

[14] Hj. Matzke, J. Chem. Soc., Faraday Trans. 2 **83**, 1121 (1987).

[15] A. B. Lidiard, J. Nucl. Mater. **19**, 106 (1966).

[16] J. Durinck (private communication).

[17] F. Garrido, A. C. Hannon, R. M. Ibberson, L. Nowicki, and B. T. M. Willis, Inorg. Chem. **45**, 8408 (2006).

[18] G. Kresse and J. Furthmüller, Comput. Mater. Sci. **6**, 15 (1996).

[19] G. Kresse and J. Furthmüller, Phys. Rev. B **54**, 11169 (1996).

[20] P. E. Blöchl, Phys. Rev. B **50**, 17953 (1994).

[21] G. Kresse and D. Joubert, Phys. Rev. B **59**, 1758 (1999).

[22] V. I. Anisimov, J. Zaanen, and O. K. Andersen, Phys. Rev. B **44**, 943 (1991).

[23] V. I. Anisimov, I. V. Solovyev, M. A. Korotin, M. T. Czyzyk, and G. A. Sawatzky, Phys. Rev. B **48**, 16929 (1993).

[24] S. L. Dudarev, D. N. Manh, and A. P. Sutton, Philos. Mag. B **75**, 613 (1997).

[25] S. L. Dudarev, G. A. Botton, S. Y. Savrasov, Z. Szotek, W. M. Temmerman, and A. P. Sutton, Phys. Status Solidi A **166**, 429 (1998).

[26] S. L. Dudarev, M. R. Castell, G. A. Botton, S. Y. Savrasov, C. Muggelberg, G. A. D. Briggs, A. P. Sutton, and D. T. Goddard, Micron **31**, 363 (2000).

[27] K. N. Kudin, G. E. Scuseria, and R. L. Martin, Phys. Rev. Lett. **89**, 266402 (2002); I. D. Prodan, G. E. Scuseria, and R. L. Martin, Phys. Rev. B **73**, 045104 (2006); **76**, 033101 (2007).

[28] H. Y. Geng, M. H. F. Sluiter, and N. X. Chen, Phys. Rev. B **72**, 014204 (2005).

[29] H. Y. Geng, N. X. Chen, and M. H. F. Sluiter, Phys. Rev. B **70**, 094203 (2004).

[30] C. Kittel, *Introduction to Solid State Physics*, 7th ed. (Wiley, New York, 1996).

[31] G. Henkelman, A. Arnaldsson, and H. Jonsson, Comput. Mater. Sci. **36**, 254 (2006).

[32] Ph. Ghosez, J. P. Michenaud, and X. Gonze, Phys. Rev. B **58**, 6224 (1998).

[33] B. Hammer, L. B. Hansen, and J. K. Norskov, Phys. Rev. B **59**, 7413 (1999).

[34] K. P. Huber and G. Herzberg, *Constants of Diatomic Molecules* (Van Nostrand, New York, 1979).

[35] William L. Jolly, *Modern Inorganic Chemistry* (McGraw-Hill, New York, 1984).

[36] G. Herzberg, Can. J. Phys. **30**, 185 (1952).

[37] M. Iwasawa, Y. Chen, Y. Kaneta, T. Ohnuma, H. Y. Geng, and M. Kinoshita, Mater. Trans. **47**, 2651 (2006).

[38] R. J. McEachern and P. Taylor, J. Nucl. Mater. **254**, 87 (1998).

[39] Here, the logic goes as that since the ordered phase $C4_2$ had not been observed in experiments but defect clusters instead; the instability of random distributed noninteracting point oxygen interstitials against the $C4_2$ phase directly supports the preference of defect clusters over the isolated interstitials.

[40] C. R. A. Catlow, Proc. R. Soc. London, Ser. A **353**, 533 (1977).

[41] H. Y. Geng, Y. Chen, Y. Kaneta, and M. Kinoshita, J. Alloys Compd. (to be published).

[42] K. Yamada, K. Kurosaki, M. Uno, and S. Yamanaka, J. Alloys Compd. **307**, 10 (2000).

[43] W. J. Weber, Radiat. Eff. **83**, 145 (1984).

[44] M. T. Robinson, J. Nucl. Mater. **216**, 1 (1994).

[45] There may be other complex mechanisms for oxygen adsorption and surface reconstruction that might considerably modify the potential surface and then the numerical values, but this picture still holds for deep layers in a qualitative sense. This argument is also supported by Ferguson and McConnell's report that about -230 kJ mol^{-1} (~ -2.38 eV) heat is released out in the chemisorption of molecular oxygen onto the surface of UO_2 during the initial stages of the reaction, as quoted in Ref. [38], which is comparable to the energy that would be released if we decompose an oxygen dimer in UO_2 matrix.

[46] C. G. Van de Walle, Phys. Rev. Lett. **80**, 2177 (1998).

[47] A. K. Cheetham, B. E. F. Fender, and M. J. Cooper, J. Phys. C **4**, 3107 (1971).

[48] A. D. Murray and B. T. M. Willis, J. Solid State Chem. **84**, 52 (1990).

[49] F. Garrido, R. M. Ibberson, L. Nowicki, and B. T. M. Willis, J. Nucl. Mater. **322**, 87 (2003).

[50] Here, no temperature influence is considered. A more realistic description should include this effect since temperature will usually alter cluster populations greatly.

[51] R. Kikuchi, Phys. Rev. **81**, 988 (1951).

[52] J. W. D. Connolly and A. R. Williams, Phys. Rev. B **27**, 5169 (1983).

[53] H. Y. Geng, M. H. F. Sluiter, and N. X. Chen, Phys. Rev. B **73**, 012202 (2006).

[54] R. A. Jackson, C. R. A. Catlow, and A. D. Murray, J. Chem. Soc., Faraday Trans. 2 **83**, 1171 (1987).

[55] Similar phenomenon also happened in cerium oxides, where the GGA+U fails to reproduce the experimental structure properties and vacancy formation energy very well within a wide range of U, indicating that there might be some slight incompatibility between the DFT+U and GGA formalism [see D. A. Andersson, S. I. Simak, B. Johansson, I. A. Abrikosov, and N. V. Skorodumova, Phys. Rev. B **75**, 035109 (2007)].